Stem Cell Research & Therapy

RESEARCH

Open Access

Ferrostatin-1 inhibits tracheal basal cell ferroptosis to facilitate the rapid epithelization of 3D-printed tissue-engineered tracheas

Cong Li[1†], Xiaoyang Zhang[1†], Haoqi Cai[2†], Kai Luo[1], Bozhong Shi[1], Bo Chen[1], Guowei Zeng[1], Jinghao Zheng[1*] and Xiaomin He[1*]

Abstract

Background Tracheal replacement is a promising approach for treating tracheal defects that are caused by conditions such as stenosis, trauma, or tumors. However, slow postoperative epithelial regeneration often leads to complications, such as infection and granulation tissue formation. Ferroptosis, which is an iron-dependent form of regulated cell death, limits the proliferation of tracheal basal cells (TBCs), which are essential for the epithelialization of tissue-engineered tracheas (TETs). This study explored the potential of ferrostatin-1 (FER-1), which is a ferroptosis inhibitor, to increase TBC proliferation and accelerate the epithelialization of 3D-printed TETs.

Methods TBCs were isolated from rabbit bronchial mucosal tissues and cultured in vitro. Ferroptosis was induced in TBCs at passage 2, as shown by increased reactive oxygen species (ROS) levels, Fe^{2+} accumulation, decreased ATP contents, and mitochondrial damage. TBCs were treated with FER-1 (1 μM) for 48 h to inhibit ferroptosis. The effects on ROS levels, Fe^{2+} levels, ATP contents, and mitochondrial morphology were measured. For in vivo experiments, FER-1-treated TBCs were seeded onto 3D-printed polycaprolactone (PCL) scaffolds, which were implanted into rabbits with tracheal injury. Epithelial regeneration and granulation tissue formation were evaluated 6 months after surgery.

Results FER-1 treatment significantly reduced ferroptosis marker levels in vitro; that is, FER-1 treatment decreased ROS and Fe^{2+} accumulation, ameliorated mitochondrial structures, and increased ATP levels. TBC proliferation and viability were increased after ferroptosis inhibition. In vivo, the group that received 3D-printed scaffolds seeded with TBCs exhibited accelerated TET epithelialization and reduced granulation tissue formation compared with the control groups. These results suggest that inhibiting ferroptosis with FER-1 improves TBC function, leading to more efficient tracheal repair.

Conclusions Ferrostatin-1 effectively inhibits ferroptosis in tracheal basal cells, promoting their viability and proliferation. This results in faster epithelialization of tissue-engineered tracheas, offering a promising strategy for improving tracheal reconstruction outcomes and reducing complications such as infection and granulation tissue formation.

†Cong Li, Xiaoyang Zhang and Haoqi Cai have contributed equally to this work.

*Correspondence:
Jinghao Zheng
zhengjh210@163.com
Xiaomin He
mrxmhe@163.com
Full list of author information is available at the end of the article

Future studies are needed to further investigate the molecular mechanisms underlying ferroptosis in TBCs and its potential clinical applications.

Keywords Tracheal basal cell, Ferroptosis, Ferrostatin-1, Tissue-engineered trachea

Background

In cases where the trachea is compromised by factors such as tumours, stenosis, trauma, or malacia, conventional surgical approaches that involve resection and end-to-end anastomosis may lead to complications such as anastomotic fistulas and tracheal rupture due to excessive tension at the anastomotic site [1–4]. In such cases, tissue-engineered tracheas, which are constructed by combining highly biocompatible scaffold materials with seeding cells, is a promising alternative treatment. However, the slow epithelialization of TETs hinders their clinical application by increasing the risk of complications, such as infection, granulation tissue formation, and early obstruction [1, 5–9]. Therefore, the timely epithelialization of biomimetic TETs remains a significant challenge in clinical application [9].

Currently, the integration of epithelial seeding cells with tissue-engineered tracheal scaffolds is one of the most effective strategies for constructing epithelialized tissue-engineered tracheas. Tracheal basal cells (TBCs), which are facultative progenitor stem cells that are located in the tracheal epithelium, are considered ideal seeding cells for the epithelialization of tissue-engineered tracheas [10, 11]. TBCs are known to have multipotent capacity to differentiate into ciliated and goblet cells [11–13]. Additionally, TBCs exhibit strong adaptability, allowing them to adhere firmly to tissue-engineered scaffolds and integrate seamlessly with scaffold materials to promote epithelialization and tissue integration; thus, TBCs are ideal seeding cells for the epithelialization of TETs [14]. However, the limited proliferative capacity of TBCs under in vitro conditions and their unstable phenotype pose significant challenges to obtaining sufficient numbers of viable cells. These limitations hinder the ability to achieve the high seeding density that is required for effective and rapid epithelialization; thus, innovative strategies are needed to increase the proliferation of these cells and maintain their regenerative capacity. To overcome these limitations, our previous research involved a novel culture strategy that used 3T3-J2 cell-derived exosomes in a coculture system to increase the proliferative capacity of tracheal basal cells, and the epithelialized tissue-engineered trachea significantly improved both short- and long-term patency rates when this strategy was applied in a tracheal defect animal model [4].

However, the exosome coculture process is complex and costly, limiting its suitability for large-scale application. This method requires stringent culture conditions, a cumbersome extraction process, and high-quality equipment, which increase the cost and complexity of this approach. Additionally, challenges in large-scale production and quality control further limit the clinical and industrial scalability of this approach. Therefore, more streamlined and cost-effective alternatives are needed to advance the field [6, 15, 16]. Our research revealed that ferroptosis may play a crucial role as a key mechanism that is involved in this process. On the basis of these findings, we suggest that the use of ferroptosis inhibitors may further increase the efficient proliferation of TBCs.

Ferroptosis is a form of programmed cell death that is driven by iron accumulation and lipid peroxidation, and it is characterized by excessive intracellular iron levels and elevated reactive oxygen species (ROS) levels, which lead to oxidative damage and cell death. In recent years, ferroptosis has been closely associated with the pathophysiology of various diseases, and it has emerged as a focal point in the study of cellular survival and metabolic regulation. In the field of stem cell research, specifically mesenchymal stem cell (MSC) and corneal stroma stem cell (NSC) research, ferroptosis has been shown to have significant impacts, and its induction severely inhibits cell proliferation and multipotency maintenance, thereby compromising regenerative potential and clinical applications [17–19]. These findings suggest that regulating ferroptosis can substantially increase stem cell viability and functionality, offering new therapeutic opportunities.

In this study, we evaluated a novel strategy for the in vitro culture of TBCs utilizing FER-1 to inhibit ferroptosis; this strategy increased cell proliferation and viability, which facilitated the rapid functional epithelialization of tissue-engineered tracheas and improved long-term patency rates after implantation.

Methods

Animals and chemical reagents

Adult male New Zealand white rabbits (4 months old, 2.0–2.5 kg) were purchased from the Shanghai Chedun Experimental Animal Raising Center (Shanghai, China). All the experimental protocols followed the appropriate guidelines and were approved by the Animal Care and Use Committee of Shanghai Children's Medical Center. The work has been reported in line with the ARRIVE guidelines 2.0. PCL raw material with

an average molecular weight of approximately 116 K, protease XIV, and collagenase type II were purchased from Sigma Aldrich (St. Louis, MO, USA). Matrigel was purchased from BD Biosciences (Bedford, MA, USA), and airway epithelial medium (PneumaCult-Ex Plus Medium) was purchased from STEMCELL Technologies Inc. (Vancouver, B.C., Canada). Trypsin was purchased from Gibco (Waltham, MA, USA). Penicillin–streptomycin solution and an EdU assay kit were purchased from Invitrogen Co. (Carlsbad, CA, USA). PBS, high-glucose DMEM, and Ham's F-12 were purchased from HyClone (Logan, UT, USA). Intracellular reactive oxygen species (ROS) production was measured with an ROS detection kit from Beyotime Biotechnology Co. (Shanghai, China). Tubulin-Tracker Deep Red was obtained from Beyotime Biotechnology Co. (Shanghai, China). Cell apoptosis was measured with an Annexin V-FITC Apoptosis Detection Kit from Vazyme Biotech Co. (Jiangsu, China). The level of intracellular chelatable iron was measured with the fluorescent probe FerroOrange from Dojindo (Kyushu, Japan). Primary antibodies against cytokeratin 5 (catalogue number A11396) were purchased from ABclonal (Wuhan, China). Ferrostatin-1 (FER-1) was purchased from Apex Bio (Houston, TX, USA). Labware consumables that were used in cell culture were purchased from Corning Life Sciences (Corning, NY, USA).

PCL scaffold design and 3D printing

The 3D-printed PCL scaffold was precisely designed to resemble a native trachea of a 4-month-old New Zealand white rabbit, as previously reported [4]. A widely used biodegradable material, namely, PCL, was used to print the scaffold. All the scaffolds were 3D printed by Beijing Advanced Medical Technologies Ltd. Inc. (Beijing, China). The Rapid Stent Fabrication System was used to prepare the scaffold. To further detect changes in chemical/material properties, the PCL raw material, 3D-printed PCL sample and irradiated sterilized 3D-printed PCL sample were analysed by Fourier transform infrared (FT-IR) spectroscopy and differential scanning calorimetry (DSC).

Isolation of autologous TBCs and FER-1 treatment

Bronchus mucosae were harvested from 6 rabbits by bronchoscopic biopsy as previously reported for further experience [4, 20]. The mucosae were repeatedly washed with PBS and incubated overnight at 4 °C with protease XIV (1 mg/mL in Ham's F-12 medium supplemented with 1% penicillin–streptomycin and amphotericin B). The digested sample was collected and filtered through a 100-μm strainer, after which the cell suspension was centrifuged at 1500 rpm for 5 min. The cells were subsequently resuspended in Ham's F-12 medium, placed in 100-mm culture dishes, and incubated at 37 °C with 5% CO_2 for 3–4 h to allow the attachment of fibroblasts. The suspended TBCs were then collected, resuspended in airway epithelial medium supplemented with 1% penicillin–streptomycin and amphotericin B (density of 1 × 10^6 cells/mL), seeded in 100-mm culture dishes that were precoated with Matrigel, and cultured at 37 °C with 5% CO_2. The expression of cytokeratin 5 (CK5) was determined by immunofluorescence staining. After expanding the tracheal basal cells (TBCs) to passage 2, the TBCs were treated with or without 1 μM FER-1 for 48 h.

Isolation of exosomes derived from 3T3-J2 cells

3T3-J2 cells were purchased from AddexBio (San Diego, CA, US) and cultured in DMEM supplemented with 10% FBS and 1% penicillin–streptomycin. After the cells reached 80% confluence, the medium was changed to fresh serum-free media for 48 h. The conditioned medium was collected and centrifuged at 2000 × g for 15 min to remove dead cells and debris. Exosomes in the conditioned medium were collected through a series of ultracentrifugation cycles as previously described [21]. The isolated exosomes were resuspended and stored at −80 °C until further use.

Cell proliferation and apoptosis assays

The proliferation and apoptosis of TBCs that were cultured with or without FER-1 at passages 0, 2, 3, and 5 were comparatively evaluated. The cell population doubling times and cell numbers at each passage were recorded to assess the different proliferation rates of TBCs in vitro. Additionally, the proliferation and apoptosis of TBCs after FER-1 treatment at each passage were evaluated.

Design and fabrication of the scaffolds

The scaffolds were formed by crosslinking fibres with a diameter of 0.25 mm, with intervals between adjacent fibres ranging from 0.2 to 0.25 mm. The length of the scaffolds in the long-axis direction was 16.5 mm, and the internal diameter of the outer layer was 6 mm. All the scaffolds were fabricated by a rapid fabrication method using a 3D multiaxis printing system at Beijing Advanced Medical Technologies Ltd. Inc. (Daxing District, Beijing, China), and polycaprolactone (PCL) was selected as the biodegradable material. The chemical properties of the PCL raw materials, 3D-printed PCL samples, and γ-irradiated scaffolds were compared by Fourier transform infrared (FT-IR) spectroscopy and differential scanning calorimetry (DSC).

Cell seeding and preculture in vitro

The preparation of the cell/hydrogel mixture, the cell seeding process, and preculture steps in vitro were conducted as described previously [21]. Specifically, the final concentration of TBCs was 5.0×10^9 cells/mL (approximately 4×10^7 cells/cm^2). After complete gelation, the scaffold was cultured in airway epithelial culture medium in a stable incubator for 7 days. The medium was replaced with fresh medium every other day.

ROS and Fe^{2+} assays

To study their ability to scavenge intracellular ROS, TBCs were seeded in 24-well plates at passages 0, 2, 3 and 5 and incubated with or without FER-1 (1 μM) for 48 h. After incubation, the cells were washed three times with PBS; then, the DCFH-DA probe (20 μM) was added, and the samples were incubated for 20 min at 37 °C, 21% oxygen, and 5% CO_2. The cells were washed three times with PBS, and the intracellular ROS levels detected by the ROS probe (DCFH-DA) were observed by confocal fluorescence microscopy (Leica SP8 confocal platform, Leica Microsystems). Similarly, the cells were stained with 1 μM FerroOrange in Hank's balanced salt solution (HBSS) for exactly 30 min at 37 °C, 21% oxygen, and 5% CO_2 and imaged immediately. Treatments were staggered to ensure a precise staining duration.

Surgical procedures

A rabbit model of tracheal epithelial injury was established by scraping the tracheal mucosa as described previously [22]. The principal operating procedures were performed by the same operator, who was blinded to the treatment group. 6 rabbits were randomized into the two groups: sham-operated control group (n = 3) and scaffold group (n = 3). All rabbits were anaesthetized with an intravenous injection of 3% pentobarbital sodium (1 ml/kg) and placed in the supine position on an operating table. Penicillin sodium was administered once by intramuscular injection to prevent infection. Each rabbit's anterior neck was shaved and disinfected. To enhance analgesia, 2% lidocaine hydrochloride was injected into the anterior neck. The trachea was exposed with a midline skin incision in the anterior neck. The incision point was located from 1.5 to 2 cm cranial to 2 cm caudal to the thyroid cartilage. The trachea was incised transversely along the tracheal cartilage between adjacent tracheal rings, with an incision length that was two-thirds of the circumference of the trachea. A nylon brush was inserted into the trachea towards the mouth, and the tracheal mucosa was completely scraped by pushing and pulling the brush against the left and right walls approximately 20 times. Adrenaline gauze was pressed into the wound to stop the seeping of the blood. The precultured cell-coated scaffolds were inserted and subsequently secured in place within the lumen of the trachea in the scaffold group. The tracheas of the rabbits in the sham-operated control group were not abraded. The muscle, subcutis, and skin were separately closed with continuous sutures. In this study, no animal samples were excluded.

Postoperative treatments

Each rabbit was individually housed and cared for to avoid potential confounders.

The observation endpoint was 6 months after surgical reconstruction, and the rabbits were sacrificed by intravenous injection of lethal dose of pentobarbital sodium (100 mg/kg). The reconstructed segmental trachea containing the TET and relevant native tissue were harvested for histological examination in batches (6 months after surgery). The obtained samples were cut into 5–7-μm sections and stained with haematoxylin and eosin (H&E) to determine their morphology. The expression of CK5 on the lumen surface of the TET was also identified by immunofluorescence staining.

Sequencing analyses of RNA transcriptomes

The RNA transcriptomes were analysed by RNA sequencing (RNA-seq). The integrity of the total RNA samples was confirmed using the Agilent RNA 6000 Nano Kit (Agilent Technologies), and the RNA integrity number (RIN) exceeded 9.0. After the removal of ribosomal RNA with the RiboMinus Eukaryote System v2 kit (Life Technologies), nondirectional RNA-seq deep sequencing libraries were constructed for the ABI/SOLiD platform utilizing the SOLiD Total RNA-seq Kit and EZ Bead (Life Technologies). The XSQ-format data produced by the SOLiD 5500XL deep sequencers (50 nt; single nondirectional reads; Life Technologies) were analysed using the RNA-seq pipeline in LifeScope (Thermo Fisher Scientific), which generated values for reads per kilobase of exon model and million mappable reads for mouse genes annotated in mm9 (UCSC Genome Browser). Uniquely mapped reads from LifeScope were assessed using fastQC (Simon Andrews, Babraham Institute) to ensure read quality and were visualized with the Integrated Genomics Viewer (Broad Institute).

Western blotting

Total proteins were extracted from cells or tissues with RIPA buffer (Beyotime, China), and the protein concentrations of the cell lysates were determined using a bicinchoninic acid (BCA) kit (Beyotime, China). The samples were separated by sodium dodecyl sulfate–polyacrylamide gel electrophoresis (SDS–PAGE) and then transferred to 0.45-μm polyvinylidene fluoride (PVDF, Millipore, USA) membranes. After being blocked with

5% skim milk powder for 2 h, the membranes were incubated with primary antibodies against ferritin heavy chain (1:1000, CST, USA), glutathione peroxidase 4 (1:1000, CST, USA), xCT (1:1000, ABclonal, China) and GAPDH (1:1000, CST, USA) at 4 °C overnight. The membranes were washed three times with TBST and incubated at room temperature with secondary antibodies for 2 h. Finally, the protein bands were visualized with an ECL luminescence reagent. Cytosolic protein levels were normalized to those of GAPDH.

Statistical analysis

All experiments were performed at least three times from different biological replicates. Numerical data are expressed as the mean ± standard deviation, and statistical analysis was performed using SPSS version 19.0. For multiple group comparisons, one-way analysis of variance (ANOVA) was utilized, and Student's t test was used to analyse significant differences between two groups. Differences were considered statistically significant at $p < 0.05$.

Results

Transcriptome sequencing (RNA-seq) analysis of TBCs and exosomes

Primary TBCs were isolated and cultured, and cell purity was determined by immunofluorescence staining for CK5 (Fig. 1a). TBCs at passage 2 (P2) displayed vacuolation and a reduced proliferative capacity. In contrast, P2 TBCs that were cocultured with exosomes remained in a healthy state and exhibited increased proliferation (Fig. 1b). Transcriptomic sequencing was performed on exosomes derived from 3T3-J2 cells, and the results confirmed the enrichment of specific RNA clusters. Transcriptome sequencing of the P2 group and the P2 + Exosome group was subsequently conducted to identify changes in gene expression. The results indicated that the ferroptosis pathway was activated in TBCs ($P < 0.05$), playing a crucial role in the coculture of TBCs with exosomes (Fig. 1c–g).

Ferroptosis occurred in tracheal basal cells

Compared with passage 0 TBCs, P2 TBCs presented extensive vacuolation, indicating significant cellular stress and compromised structural integrity. This finding suggested a decline in the cellular state and reduced proliferative capacity at this stage (Fig. 2a). Compared with passage 0 TBCs, passage 2 TBCs exhibited increased Fe^{2+} accumulation, increased ROS content, decreased ATP content, decreased proliferation, and increased apoptosis (Figs. 2b–f and 3a–c). The Western blotting results indicated that glutathione peroxidase 4 (GPX4), ferritin heavy chain (FTH) and xCT expression was decreased in passage 2 TBCs (Fig. 3d and e). These results suggest that ferroptosis occurred in the P2 group.

FER-1 alleviated ferroptosis in tracheal basal cells

Compared with those in passage 2 TBCs, the ROS contents in the P2 + FER-1, P3 + FER-1 and P5 + FER-1 groups were decreased, the Fe^{2+} accumulation was decreased, the ATP contents were increased, the numbers of cell vacuoles were decreased and the numbers of mitochondrial cristae were increased (Fig. 2a–f). The Western blotting results revealed that after FER-1 treatment, the expression levels of GPX4 and FTH in the P2 + FER-1 and P5 + FER-1 groups were greater than those in the P2 group, and the expression levels of xCT in the P2 + FER-1 group were greater than those in the P2 group; these results indicated that FER-1 inhibited ferroptosis in passage 2, passage 3, and passage 5 TBCs (Fig. 3d and e).

FER-1 promoted proliferation and decreased apoptosis in tracheal basal cells

After FER-1 treatment for 48 h, the proliferation of the cells in the P2 + FER-1 group was greater than that in the P2 group, and the proliferation in the P3 + FER-1 and P5 + FER-1 groups was greater than that in the P2 group (Fig. 3a). Annexin V/PI staining and flow cytometric analysis revealed that the percentage of apoptotic cells in the P2 group was greater than that in the P0 group. After FER-1 treatment for 48 h, the percentage of apoptotic cells in the P2 + FER-1, P3 + FER-1 and P5 + FER-1 groups was decreased compared with that in the P2 group, and the percentage of apoptotic cells in the P5 + FER-1 group was increased compared with that in the P2 + FER-1 and P3 + FER-1 groups (Fig. 3b and c).

Printing of PCL scaffolds

We carefully designed a PCL scaffold that closely resembled the dimensions of the native trachea of a 4-month-old New Zealand white rabbit. The length of the tracheal scaffold was 16.5 mm, the inner diameter was 6 mm, and the outer diameter was 6.5 mm (Fig. 4a). The layer of the scaffold consisted of vertical and horizontal PCL cross bars. The PCL cross bars had a diameter of 0.12 mm, and these cross bars simultaneously acted as a support system to strengthen the scaffold while providing enough space to coat those areas with chondrocytes. The grids of the PCL bars were 0.24 * 0.12 mm. The thermoanalytical properties, structural integrity, and mechanical characteristics of the stent showed no significant variation and were sufficient to meet the requirements for endoluminal stent implantation [4].

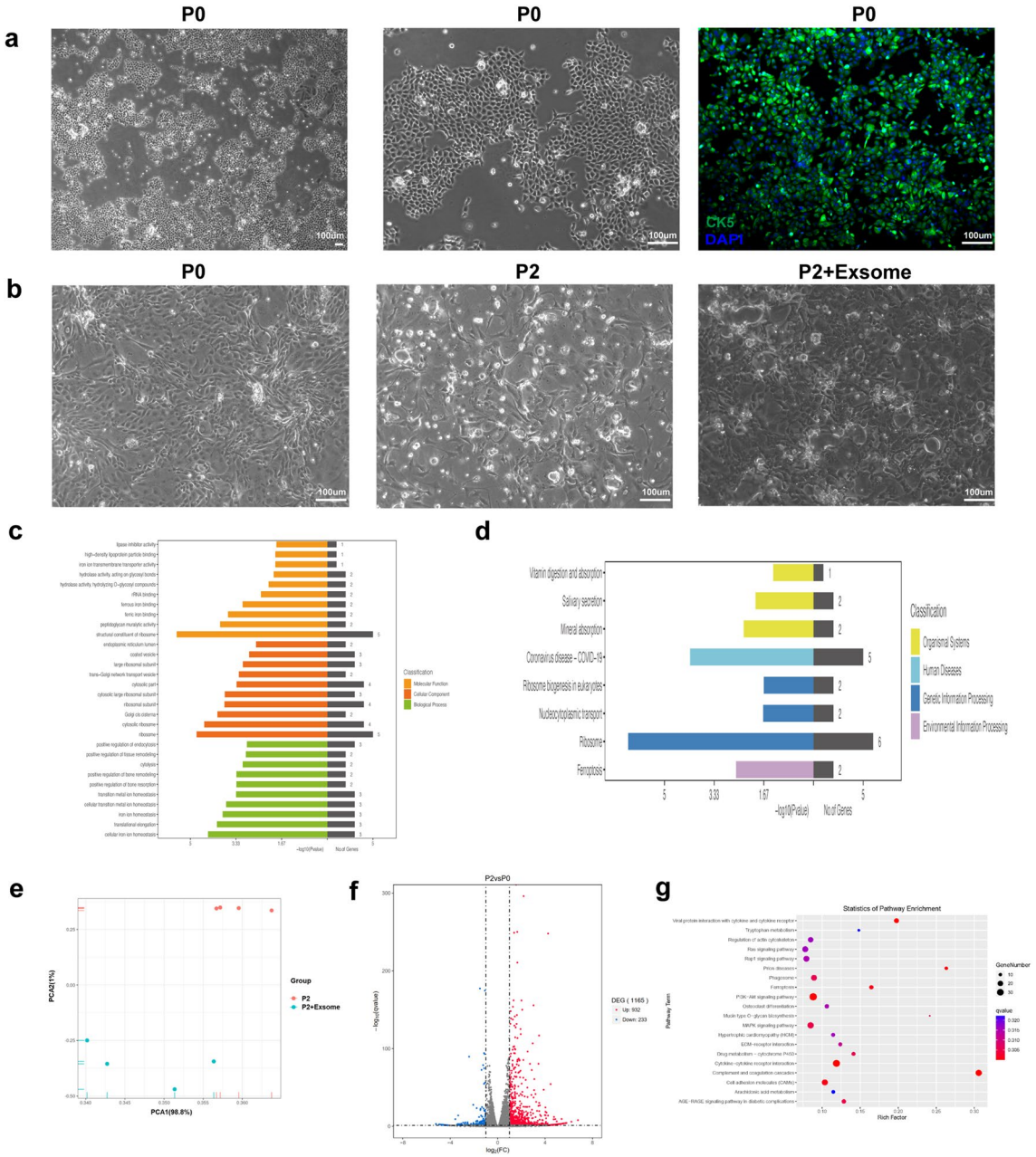

Fig. 1 Transcriptome sequencing (RNA-seq) analysis of TBCs. Representative images of primary TBCs obtained from tracheal mucosae showing typical cobblestone-like morphology under light microscopy. CK5 was highly expressed on the surface of TBCs (green: CK5, blue: DAPI-stained nuclei). **b** Representative images of TBCs at different passages under light microscopy. **c** Gene Ontology (GO) annotation analysis of exosomes from 3T3-J2 cells. **d** Kyoto Encyclopedia of Genes and Genomes (KEGG) pathway enrichment analysis of exosomes from 3T3-J2 cells. **e** Principal component analysis (PCA) for the P2 and P2 + Exsome groups. **f** Volcano plot of the differentially expressed mRNAs in the P2 and Exosome groups. **g** KEGG enrichment analysis of 1165 mRNAs

Cell seeding and preculture in vitro

After FER-1 treatment, the number and viability of TBCs in the P5 + FER-1 group were sufficient for seeding cells on the scaffolds; however, TBCs in the P2 group exhibited low proliferative activity and cell viability, and they were insufficient for cell seeding. The TBCs in the P5 + FER-1 group before cell seeding were observed under a light microscope (Fig. 4b). After 7 days of preculturing in vitro, the cell-coated scaffold was observed under a light microscope (Fig. 4b),

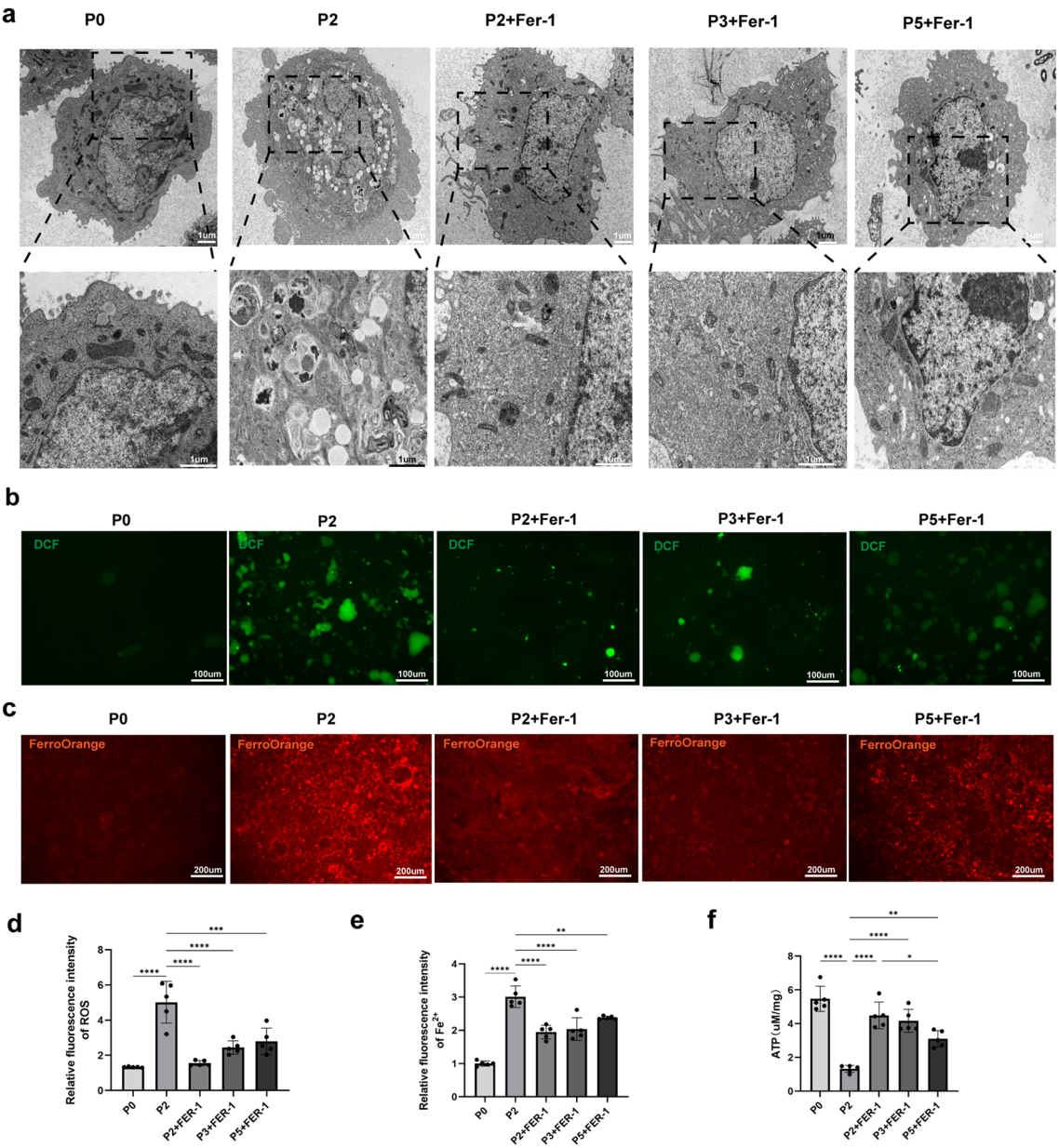

Fig. 2 Ferroptosis in tracheal basal cells. **a** Electron microscopy images showing morphological changes in the mitochondria of FER-1-treated and control TBCs at passages 0, 2, 3 and 5. **b** Representative images of intracellular ROS levels in TBCs (n = 5). **c** Representative images of intracellular Fe2 + levels in TBCs (n = 5). **d** Statistical analysis of intracellular ROS levels. **e** Statistical analysis of intracellular Fe2 + levels. **f** Intracellular ATP levels in TBCs as measured by a luminescent ATP detection assay (n = 5)

and live cell tubulin fluorescence staining by Tubulin-Tracker and nuclear staining by Hoechst 33342 were observed under a fluorescence microscope (Fig. 4c); these results confirmed the viability of the seeding cells on the scaffold after implantation. Scanning electron microscopy (SEM) examination of the cell-coated or non-cell-coated scaffolds revealed that the seeded TBCs were tightly attached to the matrix glue on the scaffolds (Fig. 4d). The adhesion of seeded TBCs on the scaffold was further verified by immunofluorescence staining of the cell-coated scaffolds (Fig. 4e).

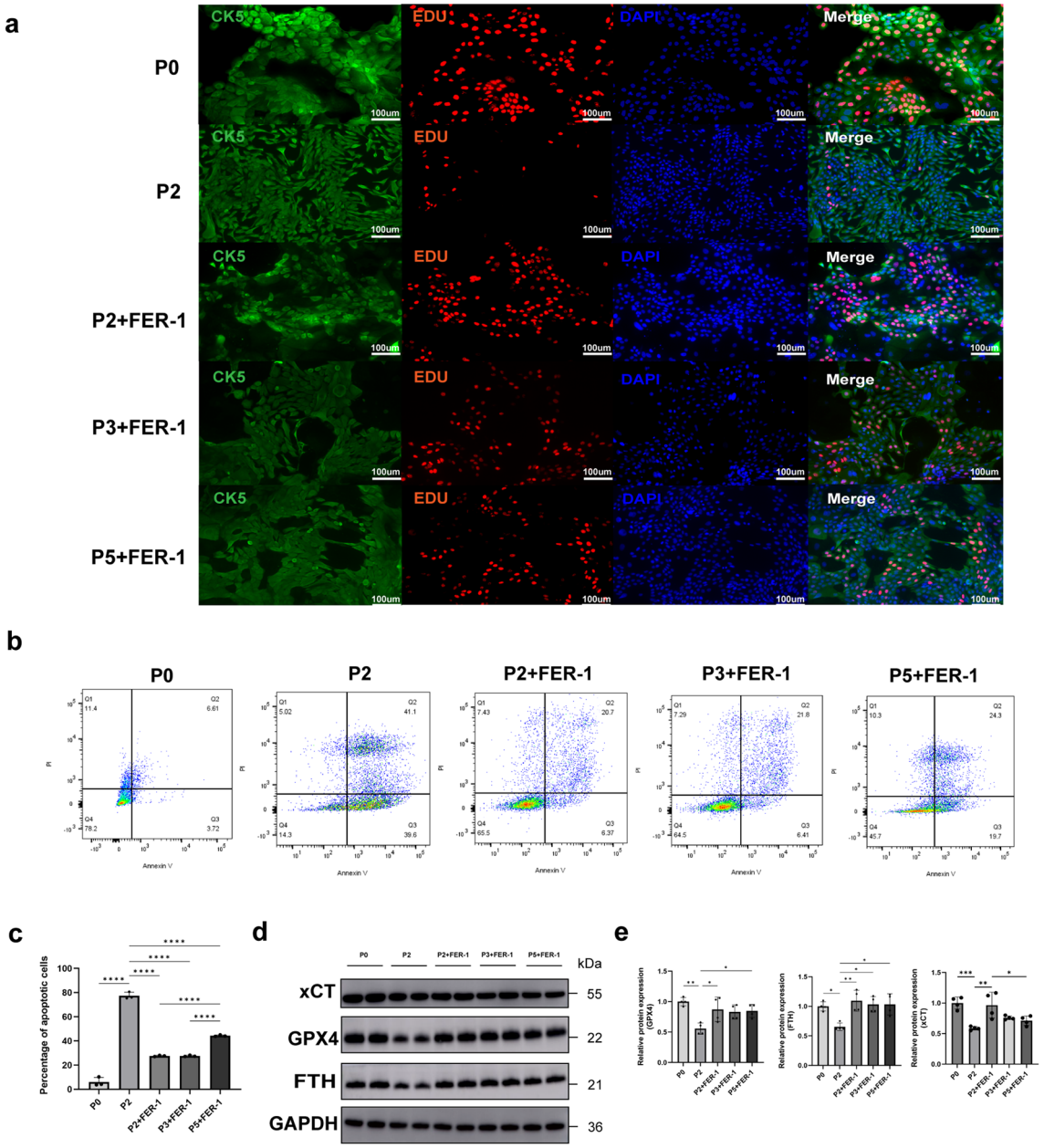

Fig. 3 Apoptosis, proliferation, and expression of ferroptosis-associated proteins in TBCs. **a** EdU assay results showing cell proliferation after FER-1 treatment (red: EdU, green: CK5, blue: DAPI). **b** Flow cytometry analysis of apoptosis of FER-1-treated and control TBCs at different passages (n = 3). **c** Statistical analysis of early and late apoptosis rates in TBCs. **d** Western blotting analysis of ferroptosis-related protein expression in TBCs. Full-length blots are presented in Supplementary Fig. 1. **e** Quantification of GPX4, FTH and xCT protein levels (n = 4)

Epithelium destruction and tracheal implantation of the scaffolds

A rabbit model of tracheal epithelial injury was established by scraping the tracheal mucosa with a nylon brush. The scaffolds with seeded cells in the P5 + FER-1 group were implanted into the trachea and anastomosed (Fig. 5a). HE staining revealed significant destruction of tracheal epithelial cells (Fig. 5b), and then, the scaffolds coated with seeding cells were implanted. Six months after surgery, tracheal re-epithelialization was observed (Fig. 5b), and no significant tracheal stenosis was observed (Video 1). Tracheal re-epithelialization was also confirmed by immunofluorescence staining for CK5 in the tissues (Fig. 5c).

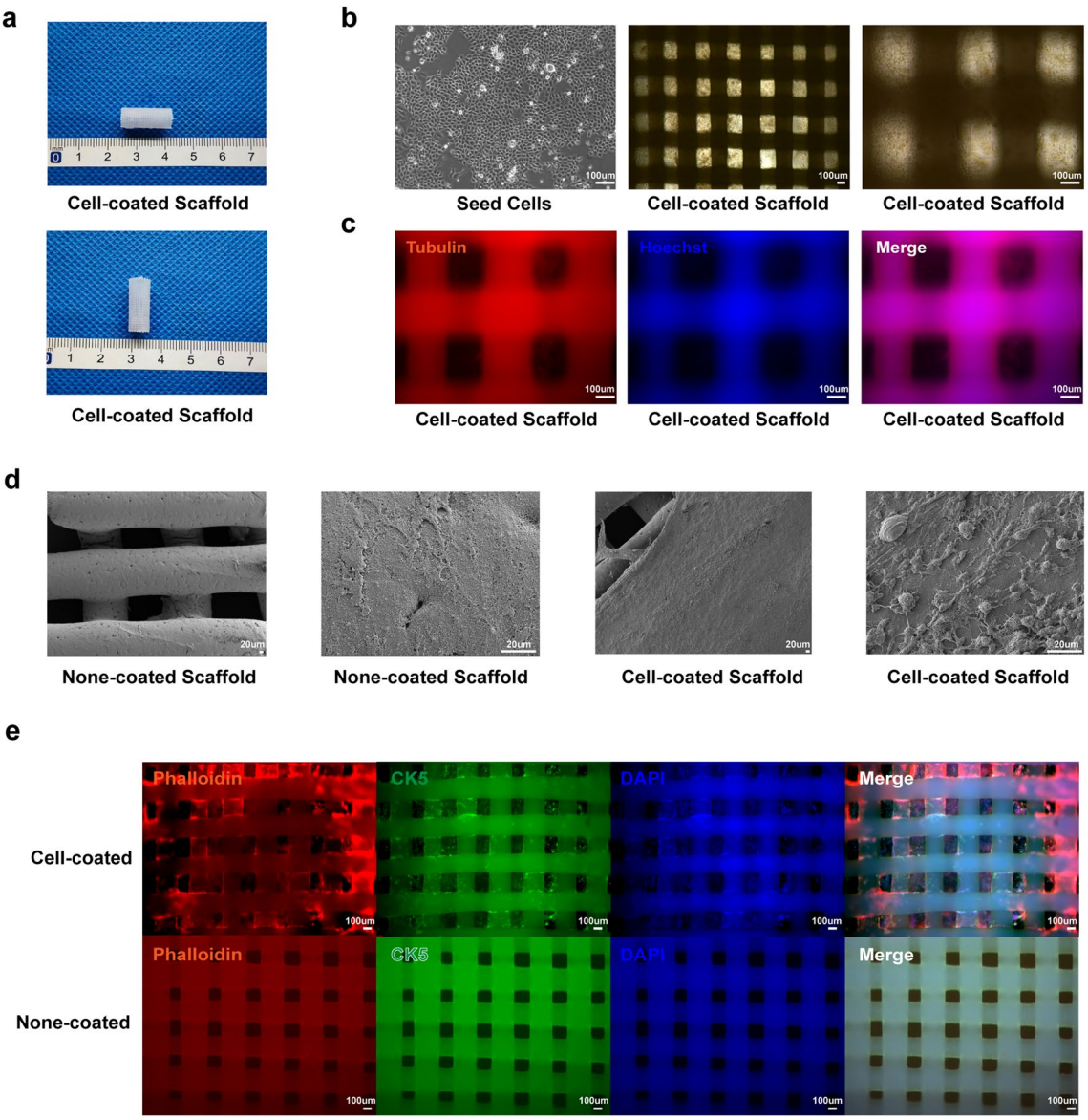

Fig. 4 Preculture of the scaffolds in vitro. **a** Gross view of cell-coated scaffolds. **b** Light microscopy images of uncoated TBCs and cell-coated scaffolds. **c** Fluorescence microscopy images showing viable cells on the scaffold surface (Red: Tubulin-Tracker, blue: Hoechst 33,342). **d** Scanning electron microscopy images of scaffolds with and without cells. **e** Immunofluorescence staining of the cell-coated scaffolds (red: Phalloidin, green: CK5, blue: DAPI)

Discussion

Currently, effective treatments for long-segment tracheal defects are lacking, and the use of tissue-engineered trachea as an alternative therapy shows promise for addressing this challenge. However, the lack of functional epithelialization leads to high rates of infection and granulation tissue formation after transplantation, causing TET dysfunction. To promote TET epithelialization, we demonstrated a promising strategy to rapidly obtain abundant and viable TBCs in vitro by adding FER-1 to TBC culture (Fig. 6). After seeding autologous TBCs onto a 3D-printed scaffold, preculturing this cell-seeded scaffold in vitro, and developing this cell-seeded scaffold in vivo, this the engineered organoid led to reconstruction of the destroyed trachea, and this scaffold rapidly achieved intact trachea epithelialization in the recipient rabbits. Rapid epithelialization allows TETs to restore tracheal barrier function by re-epithelialization, preventing early postoperative infection and granulation tissue formation. This study is the first to investigate the

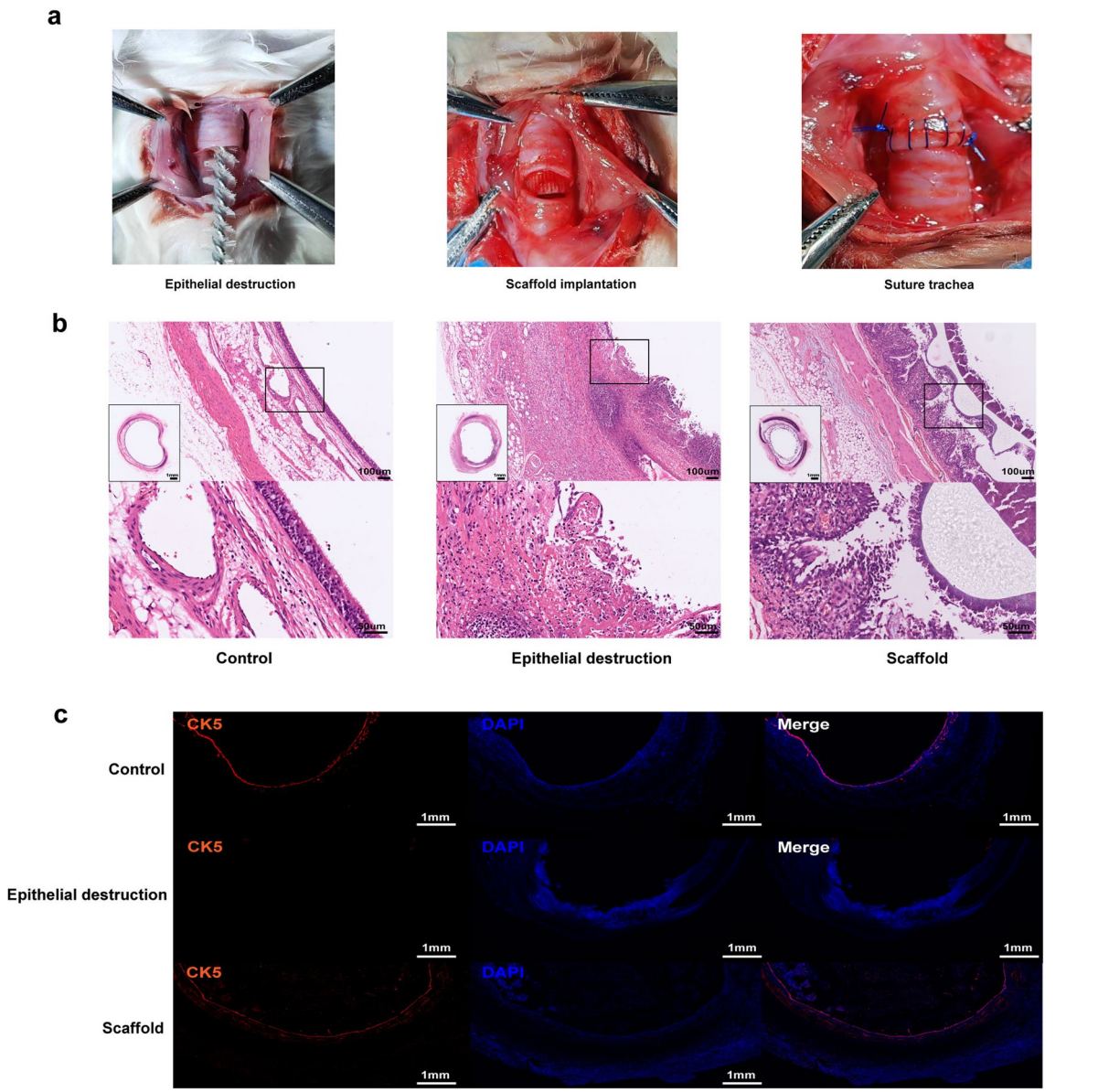

Fig. 5 Implantation of scaffolds in a rabbit epithelial injury model. **a** Surgical procedures demonstrating epithelial destruction and scaffold implantation. **b** Histological examination of tracheal epithelial tissue with H&E staining, showing epithelial destruction and re-epithelialization after implantation. **c** Immunofluorescence staining of tracheal sections for CK5 (red: CK5, blue: DAPI) showing re-epithelialization at 3 months after implantation

biological characteristics of ferroptosis in TBCs by transcriptome sequencing and to explore the regenerative effect of a new culture strategy for seeding cells on a rabbit model of epithelial destruction, demonstrating that FER-1 can inhibit ferroptosis in TBCs, promote TET epithelialization and inhibit granulation hyperplasia.

TBCs are the only cell subset in epithelial tissue with stem cell properties; they are capable of both differentiation and proliferation and play crucial roles in maintaining epithelial homeostasis and initiating rapid epithelial regeneration after tracheal injury [10, 12, 23]. As seeding cells, TBCs minimize the risk of immune rejection and postoperative complications. The strong adhesion and adaptability of these cells allow their effective integration with tissue-engineered scaffolds, promoting epithelialization and seamless tissue integration. The migratory capabilities of TBCs allow rapid coverage of damaged areas, reducing complications such as infection and granulation tissue overgrowth, which is critical for successful tracheal reconstruction. These findings suggest that TBCs are

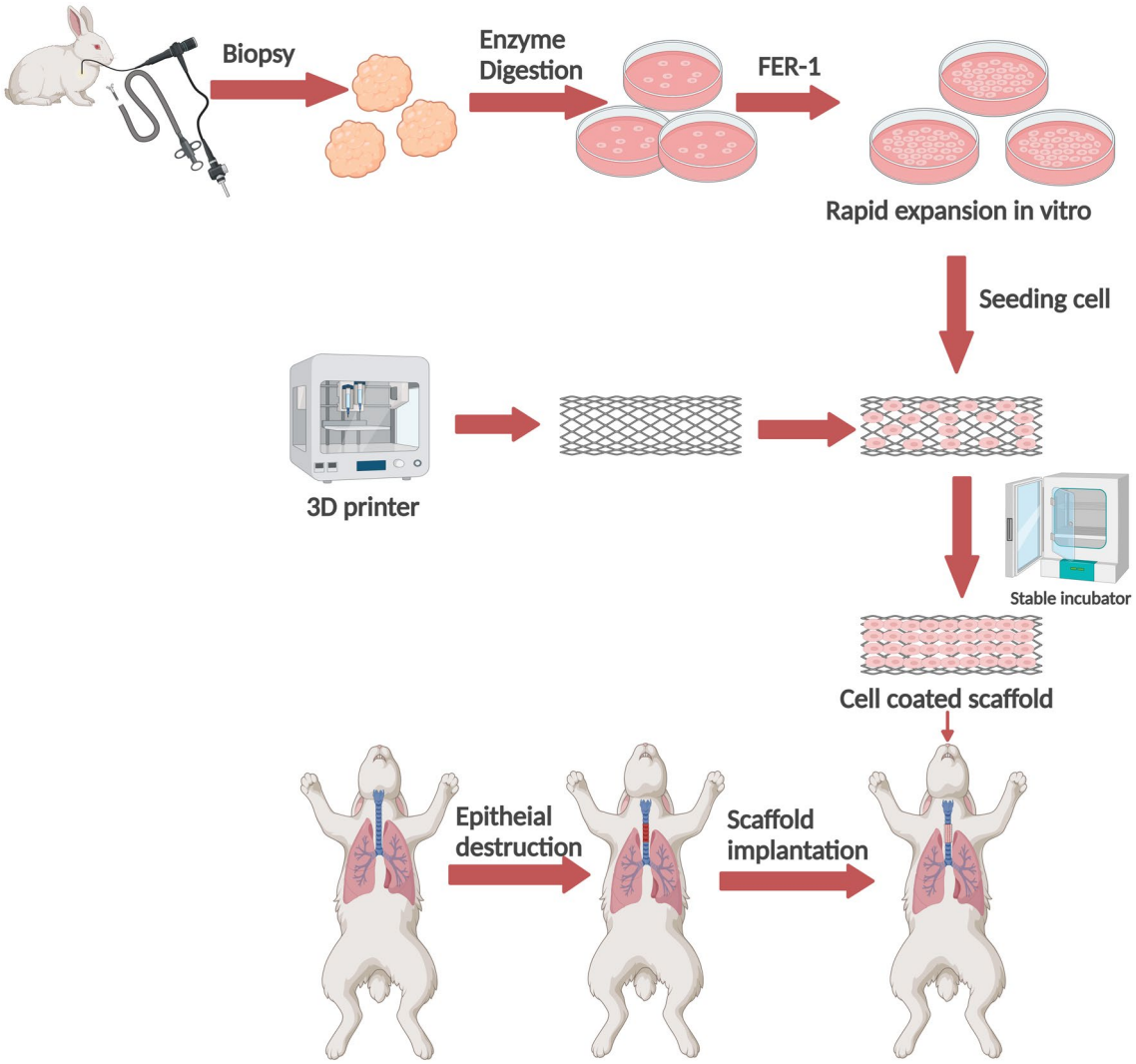

Fig. 6 Schematic diagram of 3D-printed TET scaffolds with FERF-1-treated TBCs for implantation in a rabbit model

ideal seed cells to promote the epithelialization of tissue-engineered tracheal scaffolds [12, 24].

Despite their significant role in epithelial regeneration, TBCs have some disadvantages, such as their limited proliferative capacity and their unstable phenotype under in vitro conditions, which make it difficult to obtain sufficient quantities of TBCs for the epithelialization of tissue-engineered tracheal scaffolds [4, 10]. These limitations have driven researchers to explore novel strategies to improve the expansion efficiency and viability of TBCs for therapeutic use. Similarly, our previous research revealed that more than two-thirds of single-cultured TBCs entered the late apoptotic stage even at passage 2 [4]. Moreover, these cells lost their ability to differentiate into functional ciliated tracheal epithelium, further highlighting the limitations of conventional culture methods. In contrast, the epithelialization of TET usually requires many available TBCs to achieve full coverage of the scaffolds. Owing to the limited proliferation performance of TBCs in vitro and their unstable phenotype, obtaining enough viable cells rapidly to achieve the high seeding density that is required for epithelialization is challenging. Thus, we established a new culture strategy using 3T3-J2 cell-derived exosomes in a coculture system to promote the proliferation of TBCs in vitro. The exosome coculture process is complex and expensive, making it less feasible for large-scale applications. This method demands precise culture conditions, a labour-intensive extraction process, and specialized high-quality equipment, all of which contribute to increased costs and operational complexity. As a result, there is a pressing need for more efficient and cost-effective alternatives to drive progress in the field.

In this study, our research findings suggested that the mechanism underlying the efficacy of the exosome coculture system might be associated with ferroptosis. We found that inhibiting ferroptosis in TBCs with FER-1 can increase cell proliferation, reduce apoptosis, reduce ROS production and Fe^{2+} accumulation, and increase the number and activity of seeding cells in vitro. Ferroptosis is an iron-dependent form of regulated cell death in which excess Fe^{2+} generates a large number of ROS through the Fenton reaction, resulting in the loss of cell membrane function and rupture [25, 26]. Few studies have explored the relationship between TBCs and ferroptosis. However, our study revealed that coculturing passage 2 (P2) TBCs with exosomes can alleviate ferroptosis, thereby promoting the preparation of seeding cells [27]. According to the results of in vitro cell experiments, FER-1 treatment increased the expression of GPX4 and FTH (key regulators of ferroptosis) in passage 2 TBCs, improved mitochondrial morphology, reduced ROS production and Fe^{2+} accumulation, and inhibited ferroptosis, allowing the production of enough viable TBCs for TET implantation. Additionally, compared with those in untreated cells, mitochondrial structure and function in TEM-treated cells were notably improved, with increased crista formation and increased mitochondrial activity. Furthermore, ATP functional assays demonstrated that FER-1 treatment notably increased mitochondrial functionality in TBCs, further suggesting a protective effect of FER-1 against ferroptosis-induced cellular damage. In our study, we highlighted the significant role of ferroptosis in regulating TBC activity, showing that inhibiting ferroptosis with FER-1 increased TBC proliferation, mitochondrial function, and overall cellular viability. This approach offers a novel and effective way to increase TBC expansion and prepare cells for TET applications.

Recent advances in TBC research have focused on understanding the role of TBCs in airway regeneration and repair. Key findings include the identification of signalling pathways, such as the TGF-β, BMP, and Axl pathways, that regulate TBC proliferation and differentiation [13, 28–30]. Modulating these pathways, such as by administering BMP antagonists and TGF-β inhibitors, has shown promise in increasing TBC expansion in disease models, such as COPD and tracheal injury models [13]. Additionally, cytokines such as IL-4 and IL-13, along with EGFR activation, promote TBC proliferation, particularly in inflammatory diseases [29, 31]. Unlike conventional strategies that focus primarily on modulating signalling pathways or cytokines, the ferroptosis inhibitor FER-1 increases cell activity and proliferative capacity by modulating intracellular iron ion concentrations. Previous studies have shown that TBCs typically require 7–14 days of in vitro culture, using strategies such as coculture with 3T3 cells or BMP signalling inhibitors, before being seeded onto scaffolds [4, 9, 13]. In this study, FER-1 significantly shortened the expansion time to only 7 days, accelerating TBC preparation for TET implantation while increasing cell viability and proliferation; thus, the use of FER-1 represents a more efficient and advantageous approach. In conclusion, we identified a novel, efficient, cost-effective, and rapidly applicable in vitro strategy for the expansion of TBCs. Moreover, ferroptosis inhibition facilitates rapid cell expansion, making it possible to obtain an ample supply of airway basal cells through minimally invasive procedures, such as bronchoscopic brushing, in patients with tracheal stenosis [11, 23].

In addition to the role of FER-1 in promoting tracheal epithelialization, the selection of an appropriate scaffold material is paramount to the success of TET application. In this study, PCL was chosen as the scaffold material because of its excellent biocompatibility, tunable degradation rate, and favourable mechanical properties, which make it an ideal candidate for tracheal scaffolds [32]. The slow rate of PCL degradation ensures long-term structural support during tracheal regeneration, preventing the premature loss of mechanical integrity. This allows the scaffold to maintain sufficient strength for up to 6 months, which provides ample time for tissue regeneration. Additionally, PCL can be processed using 3D printing technology to produce highly customized scaffold structures that closely resemble the anatomical and functional characteristics of the native trachea [33]. Thus, PCL not only has excellent mechanical properties and degradation kinetics but also leverages advanced manufacturing techniques, enabling the generation of patient-specific designs for optimized performance in tissue engineering applications. In our study, 6 months after implantation, bronchoscopy revealed no signs of residual fistulas, infections, or obstructions at the anastomotic site, indicating excellent stability and integration of the tracheal scaffold. These findings suggest that the scaffold maintained its structural integrity and biocompatibility, providing effective support for tracheal regeneration and function over the observation period.

To rapidly obtain abundant and viable seeding cells in vitro, we developed a promising strategy in which FER-1 was added to TBC culture. This study is the first to treat TBCs with FER-1 to inhibit seeding cell ferroptosis to promote TET epithelialization and tracheal injury treatment. This treatment achieved promising results in a rabbit model of tracheal injury, promoting airway re-epithelialization and inhibiting granulation tissue hyperplasia. However, this study has several limitations. Only

the phenotype of tracheal re-epithelialization after transplantation in vivo was investigated; the molecular mechanisms underlying cell migration and the related signalling pathways were not investigated. Additionally, there are differences in the disease course, complex epithelium defects, and composition of granulation tissue between the rabbit model and human patients. A Matrigel-only control group was not included, potentially underestimating the effect of Matrigel on epithelial repair.

Conclusions

In summary, we established a new culture strategy involving the addition of FER-1 to a coculture system of exosomes and TBCs to greatly increase the proliferation and viability of TBCs. Then, TETs that were seeded with TBCs were engineered in vitro to accelerate the epithelization of TETs and the regeneration of trachea epithelial cells in vivo. The mechanism underlying the regeneration of trachea epithelial cells and how to improve the ciliated differentiation of seeded TBCs still warrant further research in the future.

Abbreviations

TBCs	Tracheal basal cells
TET	Tissue-engineered tracheas
FER-1	Ferrostatin-1
ROS	Reactive oxygen species
PCL	Polycaprolactone
ATP	Adenosine triphosphate
MSC	Mesenchymal stem cell
CK5	Cytokeratin 5
GPX4	Glutathione peroxidase 4
FTH	Ferritin heavy chain
HBSS	Hank's balanced salt solution
H&E	Haematoxylin and eosin

Supplementary Information

The online version contains supplementary material available at https://doi.org/10.1186/s13287-025-04263-z.

Additional file1

Additional file2

Acknowledgements

The authors declare that they have not used AI-generated work in this manuscript.

Author contributions

Cong Li, Xiaoyang Zhang, and Haoqi Cai jointly developed the research design and were actively involved in conducting the experiments, analysing the data, and drafting the manuscript. The three authors engaged in in-depth discussions about data interpretation. Kai Luo contributed to the data analysis, participated in manuscript writing, and closely collaborated with Cong Li and Haoqi Cai in revising the manuscript. Bozhong Shi supported the experimental design and data collection, working with Xiaoyang Zhang to refine the experimental methodology. Bo Chen was involved in data analysis and manuscript editing, providing feedback on sections written by Haoqi Cai and Kai Luo. Guowei Zeng offered strategic guidance on the research direction and discussed the experimental design with Xiaomin He. Xiaomin He and Jinghao Zheng supervised the project, coordinated with all the authors, provided feedback on manuscript drafts, and approved the final version. They also provided the necessary financial support for the project. During the submission and revision stages, Xiaomin He substantially contributed to improving the manuscript. He played a pivotal role in refining the content, addressing reviewer comments, and enhancing the overall clarity and quality of the paper.

Funding

The author(s) disclosed receipt of the following financial support for the research, authorship, and/or publication of this article: This work was supported by the National Natural Science Foundation of China (82172101, 82072081), the Natural Science Foundation of Shanghai (23ZR1440900) and the Clinical Science and Technology Innovation Project of the Shanghai Shenkang Hospital Development Center (SHDC12021106).

Availability of data and materials

The datasets used and/or analysed during the current study are available from the corresponding author upon reasonable request. Raw RNA-sequencing files were deposited in the China National Center for Bioinformation (https://ngdc.cncb.ac.cn/): Project Accessionno. PRJCA031494.

Declarations

Competing interests

The authors declare that they have no competing interests.

Ethics approval and consent to participate

All the experiments involving animals were approved by the Ethics Committee at Shanghai Children's Medical Center (Title of approved project: Mechanistic study of circRNA_0011985 as a competing endogenous RNA (ceRNA) regulating the PGAMs/zEB1/Notch pathway to promote rapid airway epithelial regeneration; Approval number: No. SCMCIRB— K2022134-2; Date of approval: Nov. 1, 2022). In addition, all the animal procedures followed the Animal Research: Reporting of In Vivo Experiments (ARRIVE) guidelines.

Consent for publication

Not applicable.

Author details

[1]Department of Cardiothoracic Surgery, Shanghai Children's Medical Center, Shanghai Jiao Tong University School of Medicine, 1678 Dongfang Road, Shanghai 200127, China. [2]Department of Orthopedic Surgery, Shanghai Children's Medical Center, Shanghai Jiao Tong University School of Medicine, 1678 Dongfang Road, Shanghai 200127, China.

Received: 23 October 2024 Accepted: 4 March 2025
Published online: 24 March 2025

References

1. Soriano L, Khalid T, Whelan D, O'Huallachain N, Redmond KC, O'Brien FJ, et al. Development and clinical translation of tubular constructs for tracheal tissue engineering: a review. Eur Respir Rev. 2021;30: 210154.
2. Genden EM, Miles BA, Harkin TJ, DeMaria S, Kaufman AJ, Mayland E, et al. Single-stage long-segment tracheal transplantation. Am J Transplant. 2021;21:3421–7.
3. Genden EM, Laitman BM. Human tracheal transplantation. Transplantation. 2023;107:1698–705.
4. Zhang X, Jing H, Luo K, Shi B, Luo Q, Zhu Z, et al. Exosomes from 3T3-J2 promote expansion of tracheal basal cells to facilitate rapid epithelization of 3D-printed double-layer tissue engineered trachea. Mater Sci Eng C Mater Biol Appl. 2021;129: 112371.
5. Xu Y, Dai J, Zhu X, Cao R, Song N, Liu M, et al. Biomimetic trachea engineering via a modular ring strategy based on bone-marrow stem cells and atelocollagen for use in extensive tracheal reconstruction. Adv Mater. 2022;34: e2106755.
6. Xu Y, Wang Z, Hua Y, Zhu X, Wang Y, Duan L, et al. Photocrosslinked natural hydrogel composed of hyaluronic acid and gelatin enhances cartilage regeneration of decellularized trachea matrix. Mater Sci Eng C Mater Biol Appl. 2021;120: 111628.

7. Kim JH, Choi JY, Yoon HY. Comparison of three different self-expanding metal stents using rabbit models for the treatment of tracheal collapse. Acta Cir Bras. 2022;37: e370502.
8. Stocco E, Barbon S, Mammana M, Zambello G, Contran M, Parnigotto PP, et al. Preclinical and clinical orthotopic transplantation of decellularized/engineered tracheal scaffolds: a systematic literature review. J Tissue Eng. 2023;14:20417314231151824.
9. Zhu J, Lu Y, Shan Y, Yuan L, Wu Q, Shen Z, et al. Global bibliometric and visualized analysis of tracheal tissue engineering research. Tissue Eng Part B Rev. 2024;30:198–216.
10. Cole BB, Smith RW, Jenkins KM, Graham BB, Reynolds PR, Reynolds SD. Tracheal basal cells: a facultative progenitor cell pool. Am J Pathol. 2010;177:362–76.
11. Hawkins FJ, Suzuki S, Beermann ML, Barillà C, Wang R, Villacorta-Martin C, et al. Derivation of airway basal stem cells from human pluripotent stem cells. Cell Stem Cell. 2021;28:79-95.e8.
12. Ma L, Thapa BR, Le Suer JA, Tilston-Lünel A, Herriges MJ, Berical A, et al. Airway stem cell reconstitution by the transplantation of primary or pluripotent stem cell-derived basal cells. Cell Stem Cell. 2023;30:1199-216.e7.
13. Hong Y, Shan S, Gu Y, Huang H, Zhang Q, Han Y, et al. Malfunction of airway basal stem cells plays a crucial role in pathophysiology of tracheobronchopathia osteoplastica. Nat Commun. 2022;13:1309.
14. Ye YS, Chen DF, Liu M, Luo YL, Chen HJ, Zeng HK, et al. Autologous airway basal cell transplantation alleviates airway epithelium defect in recurrent benign tracheal stenosis. Stem Cells Transl Med. 2023;12:838–48.
15. Dharmadhikari S, Liu L, Shontz K, Wiet M, White A, Goins A, et al. Deconstructing tissue engineered trachea: assessing the role of synthetic scaffolds, segmental replacement and cell seeding on graft performance. Acta Biomater. 2020;102:181–91.
16. Butler CR, Hynds RE, Gowers KH, Lee Ddo H, Brown JM, Crowley C, et al. Rapid expansion of human epithelial stem cells suitable for airway tissue engineering. Am J Respir Crit Care Med. 2016;194:156–68.
17. Yuan K, Yang Y, Lin Y, Zhou F, Huang K, Yang S, et al. Targeting bacteria-induced ferroptosis of bone marrow mesenchymal stem cells to promote the repair of infected bone defects. Adv Sci (Weinh). 2024;11: e2404453.
18. Hua R, Zhao C, Xu Z, Liu D, Shen W, Yuan W, et al. ROS-responsive nanoparticle delivery of ferroptosis inhibitor prodrug to facilitate mesenchymal stem cell-mediated spinal cord injury repair. Bioact Mater. 2024;38:438–54.
19. Chen Q, Wang L, Wei Y, Xu X, Guo X, Liang Q. Ferroptosis as a potential therapeutic target for reducing inflammation and corneal scarring in bacterial keratitis. Invest Ophthalmol Vis Sci. 2024;65:29.
20. Hegab AE, Ha VL, Gilbert JL, Zhang KX, Malkoski SP, Chon AT, et al. Novel stem/progenitor cell population from murine tracheal submucosal gland ducts with multipotent regenerative potential. Stem Cells. 2011;29:1283–93.
21. Jing H, Zhang X, Luo K, Luo Q, Yin M, Wang W, et al. miR-381-abundant small extracellular vesicles derived from kartogenin-preconditioned mesenchymal stem cells promote chondrogenesis of MSCs by targeting TAOK1. Biomaterials. 2020;231: 119682.
22. Enyuan Q, Mingpeng X, Luoman G, Jinghua G, Yu L, Wentao L, et al. Erythromycin combined with corticosteroid reduced inflammation and modified trauma-induced tracheal stenosis in a rabbit model. Ther Adv Respir Dis. 2018;12:1753466618773707.
23. Rock JR, Onaitis MW, Rawlins EL, Lu Y, Clark CP, Xue Y, et al. Basal cells as stem cells of the mouse trachea and human airway epithelium. Proc Natl Acad Sci USA. 2009;106:12771–5.
24. Lynch TJ, Anderson PJ, Rotti PG, Tyler SR, Crooke AK, Choi SH, et al. Submucosal gland myoepithelial cells are reserve stem cells that can regenerate mouse tracheal epithelium. Cell Stem Cell. 2018;22:779.
25. Jiang X, Stockwell BR, Conrad M. Ferroptosis: mechanisms, biology and role in disease. Nat Rev Mol Cell Biol. 2021;22:266–82.
26. Dixon SJ, Olzmann JA. The cell biology of ferroptosis. Nat Rev Mol Cell Biol. 2024;25:424–42.
27. Zi Y, Wang X, Zi Y, Yu H, Lan Y, Fan Y, et al. Cigarette smoke induces the ROS accumulation and iNOS activation through deactivation of Nrf-2/SIRT3 axis to mediate the human bronchial epithelium ferroptosis. Free Radic Biol Med. 2023;200:73–86.
28. Tadokoro T, Gao X, Hong CC, Hotten D, Hogan BL. BMP signaling and cellular dynamics during regeneration of airway epithelium from basal progenitors. Development. 2016;143:764–73.
29. Fujino N, Brand OJ, Morgan DJ, Fujimori T, Grabiec AM, Jagger CP, et al. Sensing of apoptotic cells through Axl causes lung basal cell proliferation in inflammatory diseases. J Exp Med. 2019;216:2184–201.
30. Kiyokawa H, Yamaoka A, Matsuoka C, Tokuhara T, Abe T, Morimoto M. Airway basal stem cells reutilize the embryonic proliferation regulator, Tgfβ-Id2 axis, for tissue regeneration. Dev Cell. 2021;56:1917-29.e9.
31. Wang X, Hallen NR, Lee M, Samuchiwal S, Ye Q, Buchheit KM, et al. Type 2 inflammation drives an airway basal stem cell program through insulin receptor substrate signaling. J Allergy Clin Immunol. 2023;151:1536–49.
32. Shen Z, Sun F, Shan Y, Lu Y, Wu C, Zhang B, et al. Construction of a novel cell-free tracheal scaffold promoting vascularization for repairing tracheal defects. Mater Today Bio. 2023;23: 100841.
33. She Y, Fan Z, Wang L, Li Y, Sun W, Tang H, et al. 3D printed biomimetic PCL scaffold as framework interspersed with collagen for long segment tracheal replacement. Front Cell Dev Biol. 2021;9: 629796.

Publisher's Note